Optics Communications 287 (2013) 45–52

Contents lists available at SciVerse ScienceDirect

Optics Communications

journal homepage: www.elsevier.com/locate/optcom

Detail enhanced multi-source fusion using visual weight map extraction based on multi scale edge preserving decomposition

Jufeng Zhao, Huajun Feng*, Zhihai Xu, Qi Li, Tao Liu

State Key Lab of Modern Optical Instrumentation, Zhejiang University, Hangzhou 310027, China

ARTICLE INFO

Article history:
Received 5 December 2011
Received in revised form
21 August 2012
Accepted 21 August 2012
Available online 21 September 2012

Keywords:
Image fusion
Visual weight map
Multi scale decomposition

ABSTRACT

Image fusion is an important problem in image analysis. The abundant detail information in multisource images should be preserved or even enhanced for the fused result. In this paper, using visual weight map extraction based on multiscale edge preserving decomposition, a details enhancing fusion algorithm is proposed. The saliency extraction based visual weight map is used for image fusion at different scales, which is decomposed by edge preserving image smooth approach. With this method, the details information which human visual system interests can be preserved and enhanced easily. The quantitative comparisons of experiments demonstrate that the proposed algorithm performs better than other methods, especially in visual effect and keeping details.

1. Introduction

Image fusion is an important research topic in image processing, which includes image analysis, pattern recognition, remote sensing imaging and so on. Since image fusion makes use of multisource images with different unique informations, it has been receiving increasing attention [1,2]. For a good fusion algorithm, there are several requirements [2]. Firstly, the fused image should contain the information that the source images owns as more as possible, especially some feature information. Secondly, the fusion process should not introduce irrelevant information, such as artifacts. Thirdly, the noise should be suppressed. Finally, the result should have a good visual effect.

Many algorithms have been developed for image fusion. A dual-channel pulse coupled neural networks (dual-channel PCNN) based image fusion method is proposed [3], which is usually complicated and time-consuming, especially for multi-focus fusion. The PCA (principal component analysis) based algorithms utilize the PCA analysis to extract the main information from original images [4]. Since it would lose some information using PCA, the fusion image would lose details. Morphology based approaches may also perform well in image fusion. Bai proposed an excellent algorithm through region extraction by using multiscale center-surround top-hat transform for infrared and visible image fusion [5]. However, their fusion image quite depends on the several parameters which are difficult to select for inexperienced users. Moreover, multi-resolution approaches are the most widely used in image fusion. These kinds of methods usually decompose original image into different scale for further processing. For example, various pyramid algorithms, such as contrast pyramid [6], Laplacian pyramid [7], gradient pyramid [8], ratio pyramid [9] and morphological pyramid [10], are all utilized for image fusion. Besides, the wavelet and curvelet transform are also commonly used for fusion [11,12]. Since these methods usually utilize the multi-scale analysis for image details extraction, the disadvantage is that they may smooth some details when down-sampling and upsampling. Recently, the theory of shearlets has been studied [13]. Since the shearlet transform has the features of directionality, localization, anisotropy and multiscale, it is well applied in image fusion [2]. However, this algorithm is sometimes time-consuming.

Recently, a robust and efficient image smooth approach via L0 gradient minimization is proposed [14], with which one can easily constructed a multi-scale edge preserving decomposition. This decomposition would not make details lost as there not exist down sampling or up sampling. Moreover, saliency extraction is important in object recognition, image segmentation and adaptive compression. Researchers have applied saliency preserving in multi-focus image fusion [15]. Actually, the saliency extraction is infrequent in image fusion and still under being explored.

The proposed algorithm makes use of multi scale decomposition theory and saliency extraction. The smoothing algorithm is used to construct a multi-scale decomposition method. The saliency extraction is utilized to design a visual weight map (VWM), which defines the visual importance of each region of pixels. Different kinds of experiments show that this algorithm is suitable for image fusion. This paper is structured as follows. In Section 2, the theory of image smooth via L0 gradient minimization is introduced, and the design of VWM using saliency extraction is

* Corresponding author. Tel./fax: +86 571 87951182.
E-mail addresses: dabaozjf@gmail.com (J. Zhao), fenghj@zju.edu.cn (H. Feng).

0030-4018/$ - see front matter © 2012 Elsevier B.V. All rights reserved.
http://dx.doi.org/10.1016/j.optcom.2012.08.070

described. Image fusion algorithm using multi scale decomposition and VWM is presented in details in Section 3. Experimental results and comparison are done in Section 4. The conclusion is shown in Section 5.

2. Mathematical theory

2.1. Image smoothing via L0 gradient minimization

How to preserve edges well is an important study in image smoothing. Those algorithms which are constructed using linear filters usually would produce halo artifacts near edges. Edge preserving smoothing result could be obtained by non-linear filtering, such as bilateral filter [16] and weighted least squares [17].

A robust and efficient image smooth approach via L0 gradient minimization is proposed recently [14]. This algorithm can preserve high-contrast edges by calculating the number of non-zero gradients, which is mathematically similar to the L0 norm. For an original image I, this method tries to seek a smooth version f that is structurally similar to I, as smooth as possible everywhere except those high contrast edges in I. For each pixel p, the gradient is computed as

$$\nabla f_p = |\partial_x f_p| + |\partial_y f_p| \tag{1}$$

The gradient measurement is expressed as

$$C(f) = \#p|\nabla f_p \neq 0 \tag{2}$$

Eq. (2) counts the pixel p whose magnitude of gradient is not equal to zero. And then, the image f is defined as

$$f = \underset{f}{\operatorname{argmin}} \left\{ \sum_p (f_p - I_p)^2 + \lambda C(f) \right\} \tag{3}$$

where λ is the regularized factor. It is difficult to solve Eq. (3), which involves a discrete counting metric. In order to solve this L0-norm regularized optimization problem, an approximation is adopted. Then the optimization objective function is finally improved by introducing auxiliary variables h_p and v_p for pixel p

$$(f,h,v) = \underset{f,h,v}{\operatorname{argmin}} \left\{ \sum_p (f_p - I_p)^2 + \lambda C(h,v) + \alpha \left[(\partial_x f_p - h_p)^2 + (\partial_y f_p - v_p)^2 \right] \right\} \tag{4}$$

where h_p and v_p are corresponding to $\partial_x f_p$ and $\partial_y f_p$, and $C(h,v)=\#\{p|\ |h_p|+|v_p| \neq 0\}$, α is an automatically adapting factor to control the similarity between (h,v) and the corresponding gradient $(\partial_x f_p, \partial_y f_p)$. When α is a large enough, Eq. (4) approaches Eq. (3). After these approximations, Eq. (4) can be well solved with alternatively minimizing f and (h,v) using iterative method.

Good smooth results with edge details preserving can be obtained through optimizing Eq. (4). The parameter α is adaptively changed for ith iteration

$$\alpha_i = \alpha_0 \kappa^i, \alpha_i \leq 10^4 \tag{5}$$

According to experiments, α_0 and κ are fixed as 3λ and 2, respectively, which is a little different from Ref. [14]. And then, the only parameter needs to set is the regularized factor λ. We express the smoothed result f as the function of original image I and parameter λ for short, instead of complicated expression like Eq. (4).

$$f = S(I,\lambda) \tag{6}$$

As λ increases, the output image f becomes smoother. Typically, it is within the range [0.001, 0.1].

2.2. Visual weight map using saliency extraction

According to theory of psychology, human visual system (HVS) is sensitive to contrast of image, such as intensity and color difference. One can utilize this character of HVS to design a saliency weight map that mirrors the visual importance of each

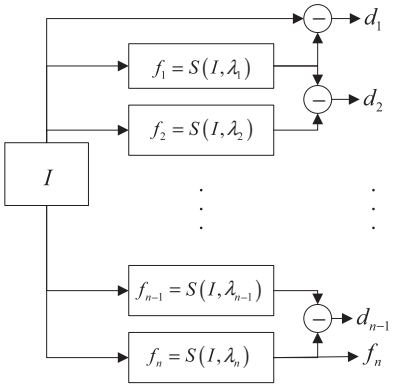

Fig. 3. The $(n+1)$-level multi-scale decomposition.

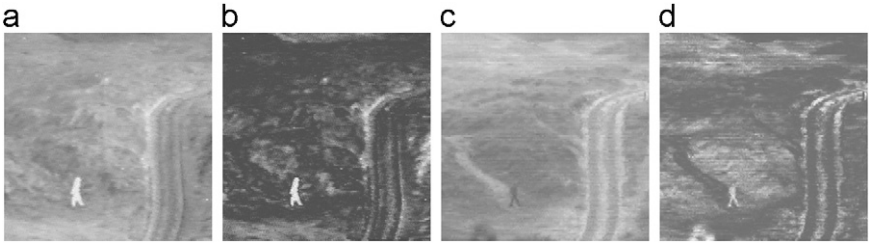

Fig. 1. Examples of VWM extraction. (a) Original image 1, (b) VWM of (a), (c) Original image 2, and (d) VWM of (c).

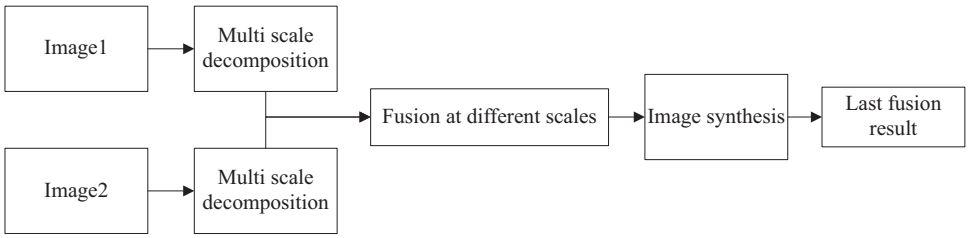

Fig. 2. Flowchart of the proposed approach.

region of pixels for original image. This kind of map is designed with saliency extraction, using the intensity contrast between different pixels of image. The saliency value of pixel p in image I is defined as

$$V(p)=\sum_{\forall q\in I}G(p,q) \tag{7}$$

where q is an arbitrary pixel of image I. The saliency value is obtained by measuring the intensity distance in Eq. (7), which is similar to the color distance metric [18]. Let I_p denote the intensity value of pixel p, then $G(p, q)$ can be expressed as the corresponding difference of pixel values in image I:

$$G(p,q)=|I_p-I_q| \tag{8}$$

According to this equation, V_p can expanded pixel by pixel by the following form

$$V(p)=|I_p-I_1|+|I_p-I_2|+\cdots+|I_p-I_M| \tag{9}$$

where M is the number of pixels in I. According to Eqs. (8) and (9), when the pixel intensity values are the same, their saliency values are equal. Take gray image for example, for intensity I_p of image I, one can easily conclude the corresponding saliency value

$$V(I_p)=\sum_{j=0}^{L-1}N_jF(I_p,j) \tag{10}$$

where j represents the intensity. N_j is the total number of pixel intensity j in image I. And L is the gray level, which equals 256 for 8-bit gray image.

Computing all the intensity value using Eq. (10), we can obtain a saliency map for original image I. The finally visual weight map (VWM) V_I is the normalized form of the saliency map, which means $V_I\in(0, 1)$. This VWM reflects the weight distribution of interests of HVS upon original image I, that is why we call the V_I visual weight map. Fig. 1 shows an example of VWM of two images. Fig. 1(a) and (c) are the original images, the corresponding VWMs of which are shown in (b) and (d), respectively.

3. Image fusion algorithm

The proposed fusion algorithm applies L0 gradient minimization based edge-preserving idea for multiresolution decomposition. At each decomposition level, images are fused using the corresponding VWM. And fused results in different scales are synthesized with different synthetic weights, result in details enhanced. The details of the implementation of the proposed approach are described in Fig. 2.

3.1. Multi scale decomposition based on image smoothing

With the help of image smoothing method mentioned in Section 2.1, a multi-scale decomposition can be easily constructed. One can design detail preserving multi-scale decompositions at a variety of scales. For an original image I, this method tries to

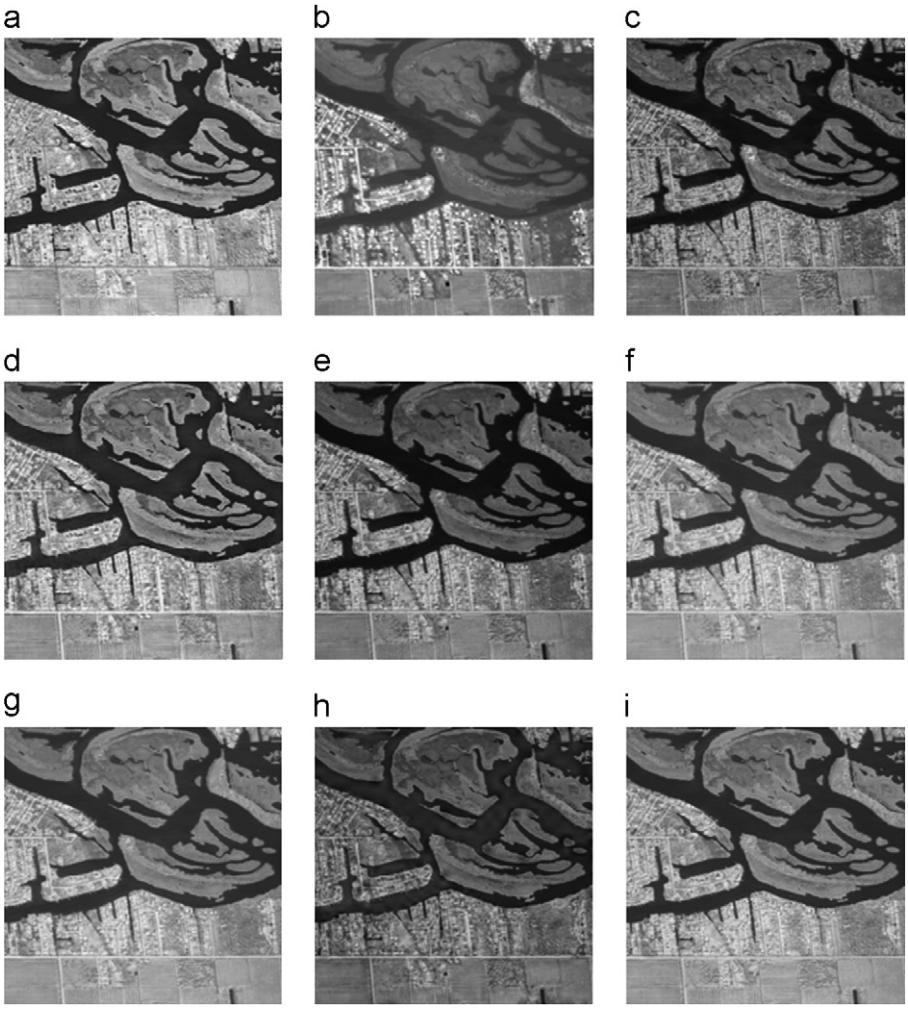

Fig. 4. Fusion results on remote sensing images. (a) Original image 1, (b) Original image 2, (c) A's result, (d) B's result, (e) C's result, (f) D's result, (g) E's result, (h) F's result and (i) G's result.

transform the image into multi-scale representation as shown in Fig. 3. This decomposition is supposed to be $(n+1)$ levels, including a base layer and n detail layers. The ith $(i=1, 2\ldots n)$ scale smoothing image is defined using Eq. (6).

$$f_i = S(I,\lambda_i) \tag{11}$$

λ_i denotes the regularized parameter for ith level smoothing, and $\lambda_i > \lambda_{i-1}$. f_n is considered as base layers, the detail layers can be defined as

$$d_i = f_{i-1} - f_i \tag{12}$$

where $f_0 = I$. In a word, this decomposition just simply decomposes the original image into base layer f_n and detail layers d_i as follows

$$\begin{aligned} I &= (f_0 - f_1) + (f_1 - f)_2 + \cdots + (f_{n-1} - f_n) + f_n \\ &= f_n + \sum_{i=1}^{n} (f_{i-1} - f_i) = f_n + \sum_{i=1}^{n} (d_i) \end{aligned} \tag{13}$$

Since the smooth based multi-scale decomposition does not do any down sampling or up sampling, thus the results are not band-limited. And this decomposition enhances image details when synthesizing with proper synthetic weight, which is advantageous in image fusion.

3.2. Image fusion using visual weight map

As VWM is defined for arbitrary image as described in Section 2.2, we utilize it for various layers fusion at different scale levels. Actually, if the pixel value is larger in VWM, HVS would pay more attention to this position. The regions with large values in VWM are usually corresponding to edge and texture areas, whose information are useful and necessary for fusion.

With multi-scale decomposition for two original images X and Y, the fusion is done in each scale level using VWM. Let d_i^X and d_i^Y denote the ith detail layers from two source images, the corresponding fused image F_i is defined as

$$F_i = \frac{(d_i^X V_X^i + d_i^Y (1 - V_X^i)) + (d_i^X (1 - V_Y^i) + d_i^Y V_Y^i)}{2} \tag{14}$$

where $i=1, 2\ldots n$, V_X^i and V_Y^i are the VWM for detail layer d_i^X and d_i^Y.

For base layer X_n and Y_n with the corresponding VWM V_X^n and V_Y^n, the fusion result F_{n+1} is calculated by

$$F_{n+1} = \frac{(X_n V_X^n + Y_n (1 - V_X^n)) + (X_n (1 - V_Y^n) + Y_n V_Y^n)}{2} \tag{15}$$

For both detail layers and base layer, the pixels and regions HVS interests are given large weights for image fusion, which make the fusion results better.

3.3. Details enhanced image synthesis

The fusion process is well done at different scales using VWM. Finally we should synthesize these fusion results. Since the original images are decomposed using Eq. (13), we try to combine the layer fusion results with various synthetic weight for details enhancement. The image synthesis criterion is designed as follows:

$$F = \beta_1 F_1 + \beta_2 F_2 + \ldots + \beta_{n+1} F_{n+1} = \sum_{j=1}^{n+1} \beta_j F_j \tag{16}$$

where F is the last fusion result, β_j $(j=1, 2 \ldots n+1)$ are the synthetic weights. Utilizing proper β_j, the visual effect of the fusion image becomes better as details enhanced.

The constants β_j $(j=1, 2 \ldots n+1)$ are used to adjust the relative weights for fusing different layers. Usually, n is small, and $n < 5$. The parameters affect the result as follows. If j is close to 1, a big β_j has more effect on enhancing the image details; otherwise it will show more effect in smoothing the result relatively. Therefore, proper weights β_j could help enhance details and suppress noise or artifacts. The β_j is selected within [0,1].

4. Experimental results and analysis

The proposed algorithm is compared with several widely used and novel excellent fusion methods, which are shearlets based method [2], multi scale center-surround top-hat transform based algorithm [5], saliency preserving method [15], the direct average algorithm, wavelet based method, PCA based algorithm. The first three are excellent fusion algorithms, and the last three are widely used methods. The image pairs for experiments include remote sensing images, medical images, infrared and visible images.

4.1. Parameters setting

The parameters we need to set include the scale level n and the regularized factors λ_i $(i=1, 2 \ldots n)$ in Section 3.1, the synthetic weight β_j $(j=1, 2\ldots n, n+1)$ in Section 3.3.

In our experiments, $n=3$ is enough. Then, for λ_j $(i=1, 2, 3)$, we finally select {0.0005, 0.003, 0.018}. The synthetic weights in Section 3.3 are selected as $\beta_j = \{0.8, 0.6, 0.6, 0.5\}$ $(j=1, 2, 3, 4)$.

Those parameters usually are fixed for fusion, although the applications are different. For all these experiments, one only need to input the original images, the algorithm automatically and rapidly gives out a good result.

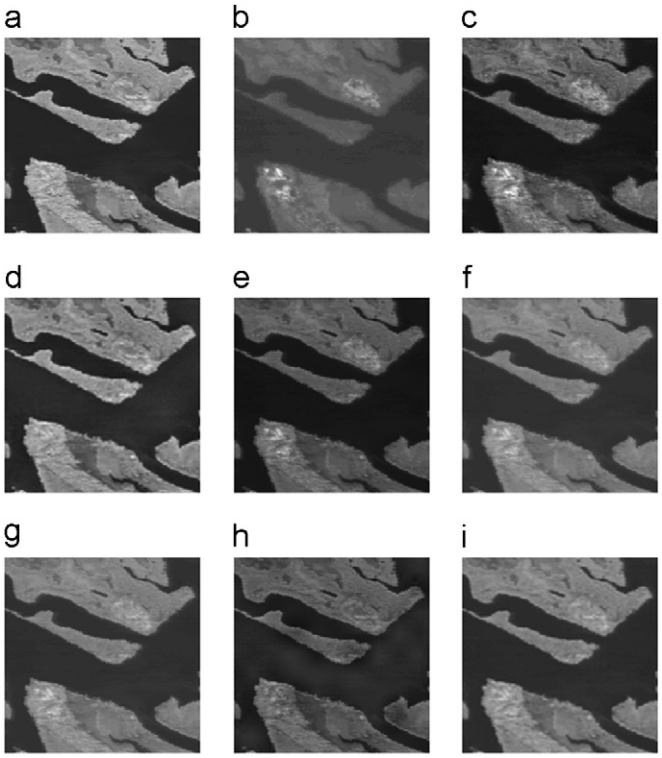

Fig. 5. Zoomed results of center parts of Fig. 4. (a) Original image 1, (b) Original image 2, (c) A's result, (d) B's result, (e) C's result, (f) D's result, (g) E's result, (h) F's result, and (i) G's result.

4.2. Image quality assessment for fusion image

To judge whether the fused result is good, HVS could immediately give out evaluation. Moreover, objective measures are also need to evaluate fused images.

We denote the two original images and the fused result by *X*, *Y* and *F*, respectively.

4.2.1. Entropy (E)

Entropy can reflect the information of image [5,19]. The entropy of fused image is defined as

$$E = -\sum_{i=0}^{L-1} p_F(i)\log_2(P_F(i)) \tag{17}$$

where L is the gray level of the image, for example $L=256$ for 8-bits gray image. $P_F(i)$ represents the probability of gray value i in image F. The larger the entropy is, the better the result is.

4.2.2. Joint entropy (JE)

The joint entropy is used to quantify the information contained between fusion image F and the two original images X and Y [5,20]. The joint entropy is computed as

$$JE_{FXY} = -\sum_{i=0}^{L-1}\sum_{j=0}^{L-1}\sum_{k=0}^{L-1} p_{FXY}(i,j,k)\log_2(p_{FXY}(i,j,k)) \tag{18}$$

$P_{FXY}(i, j, k)$ is the joint probability when gray values are i, j, k in F, X, Y, respectively. If the value of joint entropy is larger, the fused result is better.

4.2.3. Standard deviation (STD)

Standard deviation is usually used for evaluating the image clearness, which is defined using dispersion degree between gray values and the gray mean value [2].

$$STD = \sqrt{\sum_{i=1}^{N-1}\sum_{j=1}^{M-1}(F(x,y)-u_F)/MN} \tag{19}$$

where M and N are the width and height of image F, u_F is the mean value of F. The larger the *STD* is, the better the fused result is.

4.3. Visual effect comparison and quantitative comparison

All the fused results are evaluated by the *E*, *JE* and *STD* for comparison. Those algorithms are numbered as A, B, C, D, E, F, and G: A—the proposed algorithm, B—shearlets based method, C—multi scale center-surround top-hat transform based algorithm, D—saliency preserving method, E—the direct average algorithm, F—the wavelet based algorithm, and G—PCA based algorithm. For each fused image, we utilize the number to represent the corresponding algorithm for shorter, for example, "A's result" means the fusion image with the proposed method.

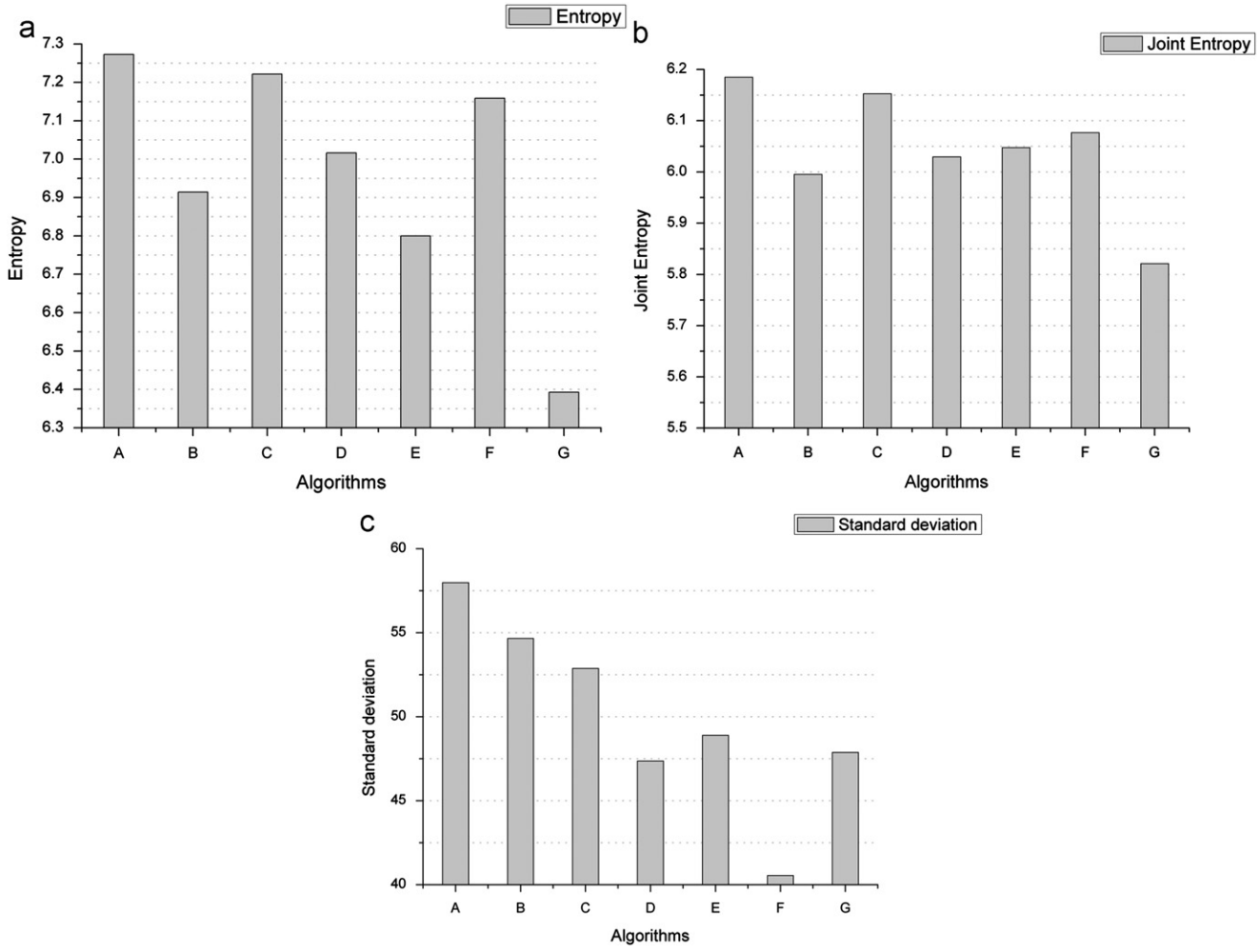

Fig. 6. Quantitative comparison using the *E*, *JE*, *STD* for remote sensing images. (a) Entropy, (b) Joint Entropy and (c) Standard deviation.

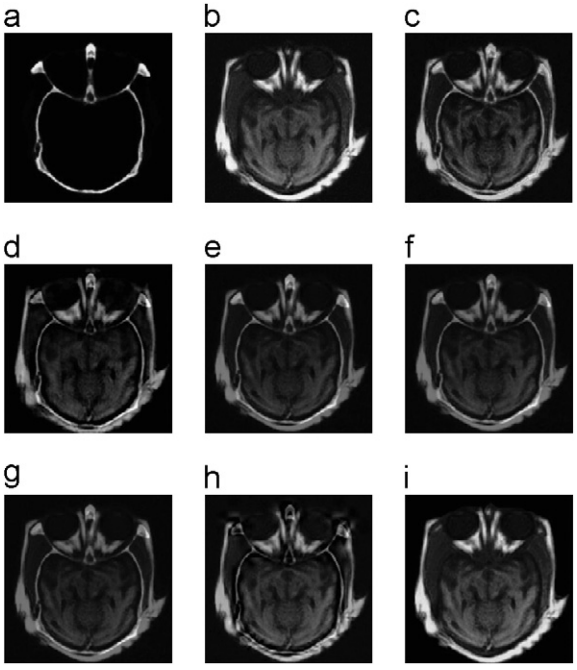

Fig. 7. Fusion results on medical images. (a) CT image, (b) MRI image, (c) A's result, (d) B's result, (e) C's result, (f) D's result, (g) E's result, (h) F's result and (i) G's result.

4.3.1. Remote sensing image fusion

The fusion images are shown in Fig. 4. Fig. 4(a) and (b) are original remote sensing images captured in different bands. The two images own their unique information, respectively. Fig. 4(c–i) are the fused results with different methods. Fig. 5 shows the local zoomed results of Fig. 4. From Fig. 5, it is obvious that the proposed algorithm gets more information from both original images. The evaluation results using *E*, *JE* and *STD* are shown in Fig. 6. From Fig. 6, we can find that proposed method obtain highest assessment in all the three measures. From Figs. and image quality evaluations, one can conclude that the proposed method performs better than other methods, both in visual effect and details preserving.

4.3.2. Medical image fusion

As shown in Fig. 7(a) and (b), the source images are CT (Computer Tomography) and MRI (Magnetic Resonance Imaging) images. The fused results using different methods are shown in Fig. 7(c–i), whose corresponding evaluation results are shown in Fig. 8. According to quantitative comparisons in Fig. 8, the wavelet performs close to the proposed method. However, from Fig. 7(h), one can find that the wavelet's result produced artifacts, which one cannot tolerate. The fusion image using the proposed algorithm has a good visual effect, preserving and enhancing unique detail information from both source images.

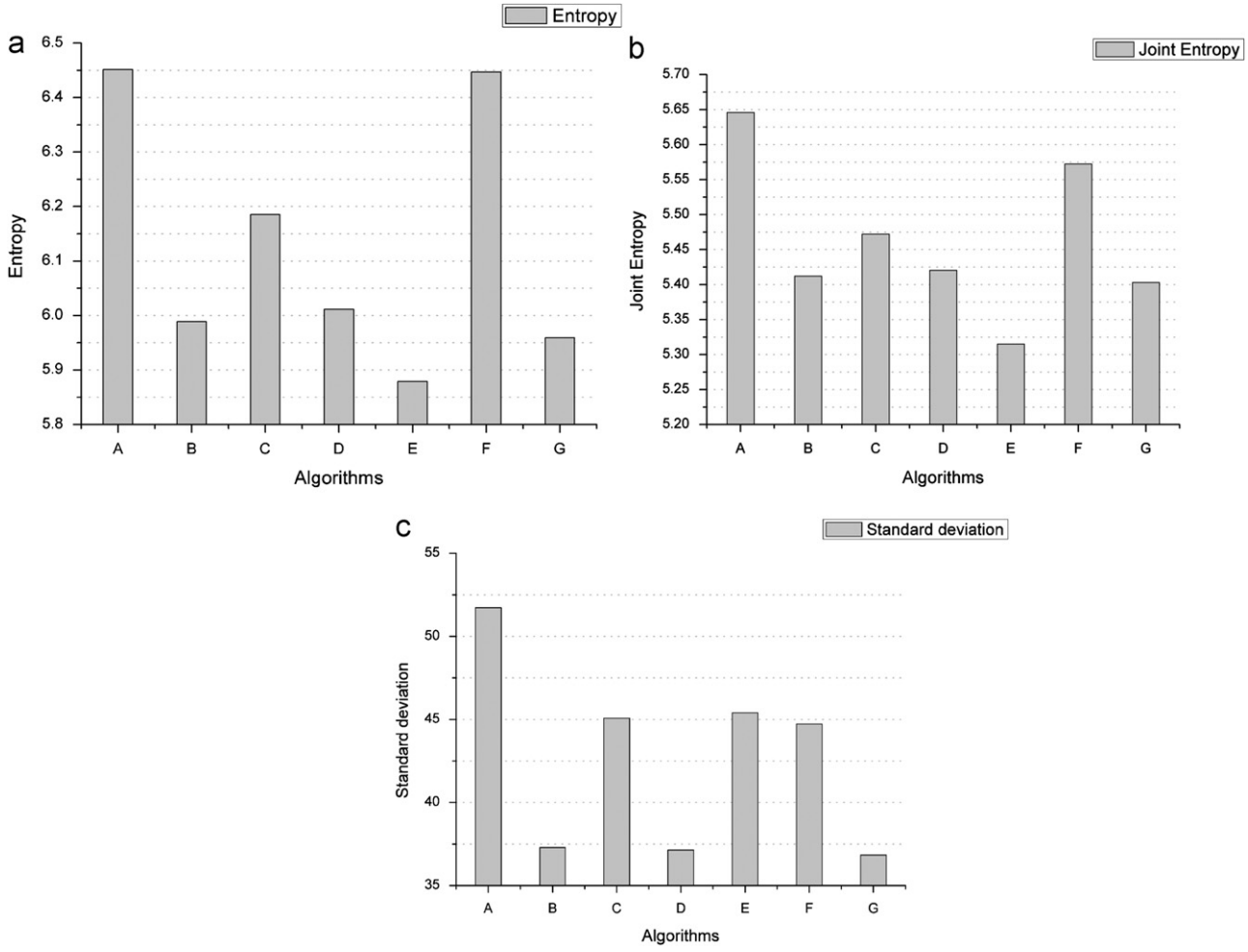

Fig. 8. Quantitative comparison using the *E*, *JE*, *STD* for medical images. (a) Entropy, (b) Joint Entropy and (c) Standard deviation.

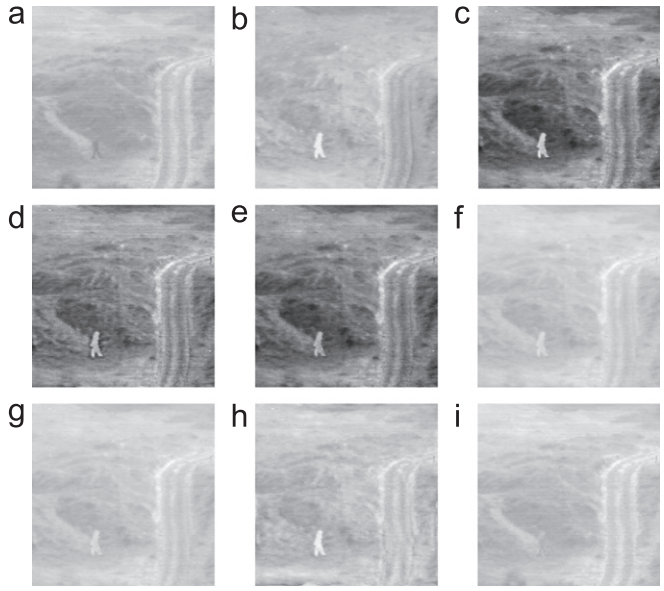

Fig. 9. Fusion results on visible and infrared images. (a) Visible image, (b) Infrared image, (c) A's result, (d) B's result, (e) C's result, (f) D's result, (g) E's result, (h) F's result and (i) G's result

4.3.3. Fusion for visible and infrared images

The two source images are visible and infrared ones, as shown in Fig. 9(a) and (b). Infrared image usually contains particular target information which one could not find in visible image. And the visible image usually has abundant object details. The information of both images should be combined together. The fused images using various approaches are shown in Fig. 9(c–i), whose image quality are evaluated by *E*, *JE* and *STD* just as shown in Fig. 10. From the visual effect and evaluation results, we can find that the proposed algorithm obtain a better fusion effect.

4.4. Further analysis

According to the experiment results, we further analyze the performance of the proposed algorithm in four aspects:

Table 1
Comparison of processing time for medical images.

Algorithms	A	B	C	D	E	F	G
Time (s)	13.44	49.35	14.89	26.38	0.01	0.79	0.19

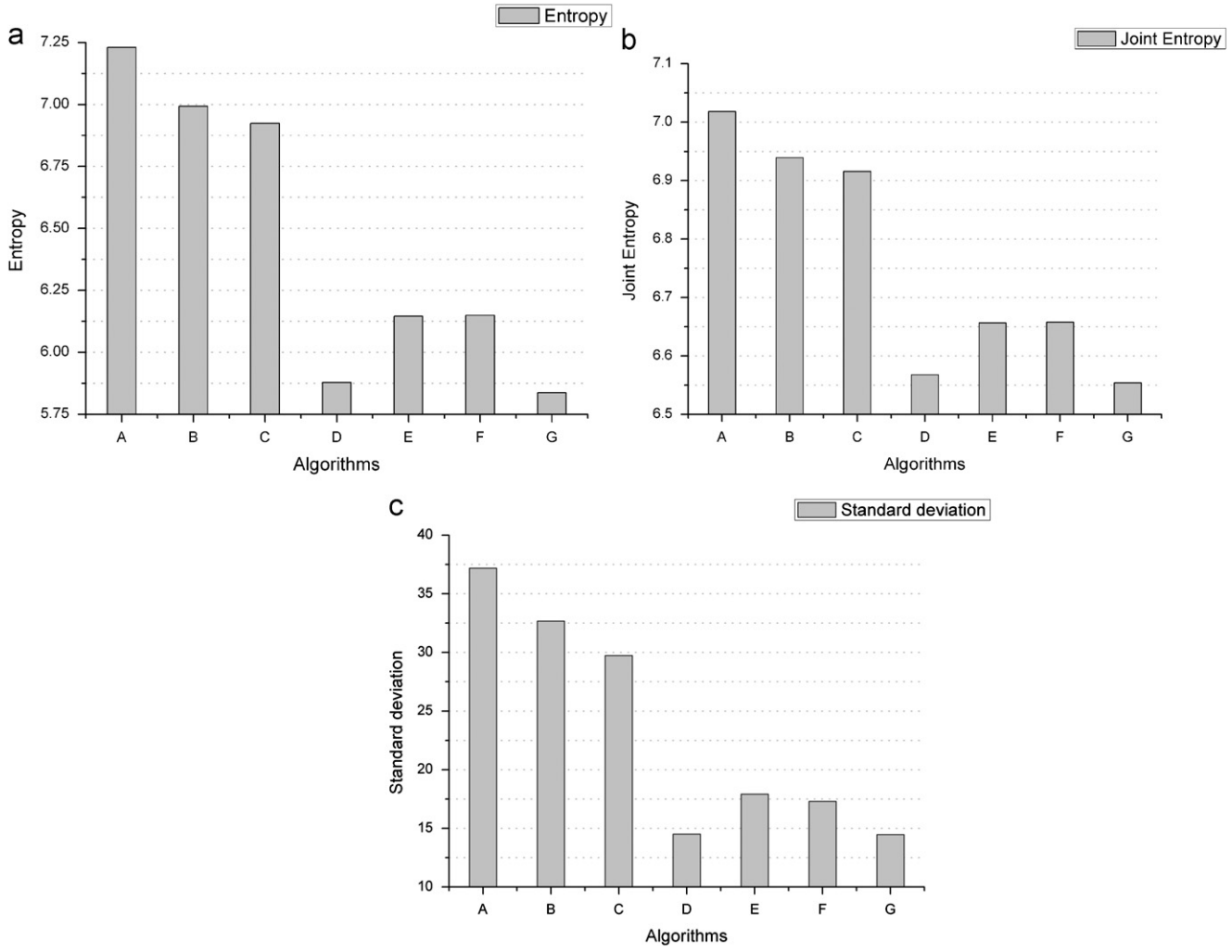

Fig. 10. Quantitative comparison using the *E*, *JE*, *STD* for visible and infrared images. (a) Entropy, (b) Joint Entropy and (c) Standard deviation.

4.4.1. Applicability and robustness

Actually, the proposed algorithm has a wide applicability, as it can be used in image fusion for remote sensing images, medical images, visible and infrared images. From Figs. 6, 8 and 10, the image quality measures prove that the proposed method performs best, working robustly and excellently in all three different applications.

4.4.2. Efficiency

Efficiency is an important index for evaluating image processing algorithms. To measure and compare the efficiency of algorithms, we adopt the medical images as shown in Fig. 7(a) and (b) for test. The medical images are gray scale images, with the size of 256×256. For all the seven methods as described in Section 4.3, the processing time is listed in Table 1. One can find that those widely used methods, such as E, F and G, work much faster than those excellent method like A, B, C and D. The shearlets based method (algorithm B) is most time-consuming, but the proposed method (algorithm A) works much faster. Comparing with algorithms E, F and G, the algorithm A is much slower, due to the multi-scale decomposition.

4.4.3. Visual effect

From the fusion result as shown in Figs. 4, 5, 7 and 9, the proposed algorithm has the best visual effect. The VWM works suitably and helpfully in image fusion, as it takes the characteristic of HVS into account. The results of shearlets based method (algorithm B) would sacrifice the contrast, because the low frequency information is just the average of the two source images. Taking the fusion of visible and infrared images for example, the results of algorithms D, E, F are not sharp or clear, and the G's result lose the "people" information from infrared image. The results of algorithms A, B and C are much better, and the A's result has the best visual effect.

4.4.4. Image details

Since we adopt the edge preserving multi scale decomposition and the details are usually enhanced using effective synthetic weights, the fused results are always abundant of detail information. Take the fusion of remote sensing images for example, the results of algorithm A contains more information. Especially for the zoomed results of center part as shown in Fig. 5, the A's result obviously inherits unique details form two original images, but most of other algorithms lose these details more or less.

5. Conclusion

How to combine the information of source images into a fused image with details preserving and a good visual effect is a significant and difficult problem. In this paper, the authors proposed an image fusion method using VWM extraction based on multi scale edge preserving decomposition. A robust image smooth algorithm is utilized to transform image into multi scale which contains detail layers and base layer. Moreover, the VWM works well in fusion at different scale levels as it is designed by using saliency extraction, which takes account of the attention of HVS. From several experiments, it is proved that the details of source images are preserved even enhanced, which makes fused result have a good visual effect. The proposed method works robustly and excellently for all the three kinds of images. The future work should be focused on the efficiency of algorithm.

Since our algorithm could do well in preserving or even enhancing image details and regions which HVS interests, the method would be suitable for target detection, pattern recognition, and other image processing fields.

Acknowledgments

We thank the reviewers for helping us to improve the paper. And we thank Dr. Li for checking the text. The original images used in this paper are downloaded from the websites www.imagefusion.org, many thanks to Alexander Toet and the TNO Human Factors Research Institute. This work is supported by the State Key Development Program of Basic Research of China (Grant no. 2009CB724006) and the National Natural Science Foundation of China (Grant no. 60977010).

References

[1] Y. Chai, H. Li, Z. Li, Optics Communications 284 (2011) 4376.
[2] Q. Miao, C. Shi, P. Xu, M. Yang, Y. Shi, Optics Communications 284 (2011) 1540.
[3] Z. Wang, Y. Ma, J. Gu, Pattern Recognition 43 (2010) 2003.
[4] M. González-Audícana, J.L. Saleta R, IEEE Transactions on Geoscience and Remote Sensing 42 (2004) 1291.
[5] X. Bai, F. Zhou, B. Xue, Optics Express 19 (2011) 8444.
[6] A. Toet, J.M. Valeton, L.J. Van Ruyven, Optical Engineering 28 (1989) 789.
[7] Z. Liu, K. Tsukada, K. Hanasaki, Y.K. Ho, Y.P. Dai, Pattern Recognition Letters 22 (2001) 929.
[8] P.J. Burt, Proceedings of the Society for Information Display (1992) 467.
[9] A. Toet, Pattern Recognition Letters 9 (1989) 245.
[10] G.K. Matsopoulos, S. Marshall, Journal of Visual Communication and Image Representation 6 (1995) 196.
[11] G. Qu, D. Zhang, P. Yan, Optics Express 9 (2001) 184.
[12] F. Nencini, A. Garzelli, S. Baronti, L. Alparone, Information Fusion 8 (2007) 143.
[13] G. Kutyniok, D. Labate, Transactions of the American Mathematical Society 361 (2009) 2719.
[14] L. Xu, C. Lu, Y. Xu, J. Jia, ACM Transactions on Graphics (SIGGRAPH Asia 2011) 30 (2011).
[15] R. Hong, C. Wang, M. Wang, F. Sun, International Journal of Innovative Computing, Information and Control 5 (2009) 2369.
[16] B. Weiss, ACM Transactions on Graphics 25 (2006) 519–526.
[17] J.A. Fessler, IEEE Transactions on Medical Imaging 13 (1994) 290.
[18] Y. Zhai, M. Shah, Proceedings of the 14th Annual ACM International Conference on Multimedia, New York, 2006.
[19] J.W. Roberts, J. Van Aardt, F. Ahmed, Journal of Applied Remote Sensing 2 (2008) 023522.
[20] G. Qu, D. Zhang, P. Yan, Electronics Letters 38 (2002) 313.